

# Characterization of the Porous Structure of SBA-15

Michal Kruk and Mietek Jaroniec\*

Department of Chemistry, Kent State University Kent, Ohio 44240

Chang Hyun Ko and Ryong Ryoo

Department of Chemistry and School of Molecular Science (BK21), Korea Advanced Institute of Science and Technology, Taeduk Science Town, Taejeon, 305-701 Korea

Received February 23, 2000. Revised Manuscript Received May 2, 2000

SBA-15 ordered mesoporous silicas were synthesized using the method reported by Zhao et al. The structures of these materials were characterized using powder X-ray diffraction (XRD), thermogravimetric analysis (TGA), and nitrogen adsorption. The samples were found to exhibit structural properties similar to those reported earlier. Our study confirmed that the size of primary mesopores of SBA-15 can be tailored by the choice of synthesis temperature and that SBA-15 exhibits a significant amount of disordered micropores and small mesopores. The volume and size of these complementary pores were found to be dependent to some extent on the synthesis/aging temperature. It was shown that the washing of as-synthesized SBA-15 in water or ethanol was accompanied by an appreciable structural shrinkage and led to the removal of a significant part of the polymeric template. Therefore, washing needs to be avoided if one wants to isolate SBA-15 without appreciable loss of the template. It was confirmed that water-washed SBA-15 samples have fully accessible primary mesopores. Ethanol-washed samples also were found to exhibit accessible porosity. Despite an appreciable content of the template in the water- and ethanol-washed samples, their pore sizes were usually larger than those of the calcined materials. The observed structural properties of SBA-15 and their dependence on the synthesis temperature and washing were attributed to the changes in the degree of penetration of the poly(ethylene oxide) chains of the triblock copolymer template within the siliceous walls of SBA-15.

## Introduction

The application of oligomers and polymers as templates in the synthesis of mesoporous silicas and other mesoporous oxides has recently attracted much attention and led to the development of convenient synthesis pathways for materials with tailored porous structures and desirable forms/particle morphologies. Many different types of oligomeric and polymeric templates have already been employed in the synthesis of mesoporous oxides. First, it was demonstrated that oligomers, such as alkyl poly(ethylene oxide) and alkylphenyl poly(ethylene oxide) surfactants, are facile supramolecular templates.<sup>1,2</sup> The use of liquid-crystalline phases of oligomeric surfactants under acidic conditions allowed for the preparation of hexagonal (pore size of about 3 nm) and cubic mesoporous silicas.<sup>1</sup> The synthesis in neutral media afforded disordered mesoporous silicas with large specific surface areas and quite uniform pores up to about 5 nm<sup>2</sup> as well as aluminas with average pore sizes up to about 8 nm.<sup>3</sup> The silicas were prepared in aqueous solutions, whereas the aluminas were obtained

in organic solvents with small addition of water. The incorporation of cerium and lanthanum ions was found to improve the stability of the aluminas.<sup>4</sup> The addition of fluoride ions and the judicious choice of the synthesis temperature allowed for tailoring the silica pore size.<sup>5</sup> The presence of fluoride ions was also found to facilitate the synthesis,<sup>5,6</sup> allowing one to perform it in more dilute solutions.<sup>6</sup> The addition of sodium salts in neutral media afforded silicas with bimodal mesoporous systems,<sup>7</sup> and the addition of some other salts introduced the long-range hexagonal or cubic ordering.<sup>8</sup> Acidic media were found suitable for the synthesis of cubic and hexagonal silicas,<sup>9</sup> whereas both acidic and basic media allowed for the incorporation of heteroatoms in the silica structure.<sup>10</sup> The postsynthesis hydrothermal treatment of as-synthesized oligomer-templated silicas in water was found to result in the pore size increase and improvement in the uniformity of the disordered struc-

\* To whom correspondence should be addressed. E-mail: Jaroniec@columbo.kent.edu; phone: (330) 672 3790; fax: (330) 672 3816.

(1) Attard, G. S.; Glyde, J. C.; Goltner, C. G. *Nature* **1995**, *378*, 366.  
(2) Bagshaw, S. A.; Prouzet, E.; Pinnavaia, T. J. *Science* **1995**, *269*, 1242.  
(3) Bagshaw, S. A.; Pinnavaia, T. J. *Angew. Chem., Int. Ed. Engl.* **1996**, *35*, 1102.

(4) Zhang, W.; Pinnavaia, T. J. *Chem. Commun.* **1998**, 1185.  
(5) Prouzet, E.; Pinnavaia, T. J. *Angew. Chem., Int. Ed. Engl.* **1997**, *36*, 516.  
(6) Voegtlin, A. C.; Ruth, F.; Guth, J. L.; Patarin, J.; Huve, L. *Microporous Mater.* **1997**, *9*, 95.  
(7) Bagshaw, S. A. *Chem. Commun.* **1999**, 1785.  
(8) Zhang, W.; Glomski, B.; Pauly, T. R.; Pinnavaia, T. J. *Chem. Commun.* **1999**, 1803.  
(9) Zhao, D.; Huo, Q.; Feng, J.; Chmelka, B. F.; Stucky, G. D. *J. Am. Chem. Soc.* **1998**, *120*, 6024.  
(10) Bagshaw, S. A.; Kemmitt, T.; Milestone, N. B. *Microporous Mesoporous Mater.* **1998**, *22*, 419.

ture,<sup>11</sup> or even in transformation from the disordered to hexagonal structure.<sup>12</sup> The aforementioned synthesis procedures employed tetraethyl orthosilicate (TEOS) or tetramethyl orthosilicate, but the synthesis of mesoporous silicas was also possible when cheap and convenient silica sources, such as sodium silicate or H<sub>2</sub>SiF<sub>6</sub>, were employed.<sup>13,14</sup> Oligomeric templates were found suitable for the preparation of mesoporous spherical silica particles of the size suitable for chromatographic applications,<sup>15</sup> silica thin films,<sup>16,17</sup> and spherical nanoparticles of vesicular, hexagonal, or cubic structures.<sup>17,18</sup> Moreover, oligomeric surfactants were shown to be facile templates for the synthesis of functionalized mesoporous silicas via co-condensation of TEOS with organotriethoxysilanes<sup>19</sup> and for the preparation of mesoporous titanium oxo phosphate.<sup>20</sup> In addition to the aforementioned oligomeric surfactants, ethoxylated sorbitan esters were found useful in the synthesis of ordered<sup>9</sup> and disordered mesoporous silicas.<sup>21</sup>

Liquid-crystalline phases of neutral diblock copolymers (such as polystyrene–polybutadiene and polybutadiene–poly(ethylene oxide)), as well as cationic and anionic diblock copolymers in acidic media, were also successfully used to template mesoporous silicas.<sup>22–28</sup> In this way, monolithic materials with channel-like pores of size up to about 8 nm were synthesized.<sup>22,23</sup> Silicas with large spherical pores (diameter of 10–50 nm),<sup>24,25</sup> hexagonally ordered cylindrical pores,<sup>25,26</sup> and lamellar/vesicular structures stable upon calcination<sup>26</sup> were also obtained. Diblock copolymer templating was also combined with polymer latex templating to obtain mesoporous silicas with bimodal pore size distributions.<sup>27</sup> In addition, the preparation of metal nanoparticles inside the copolymer micelle cores allowed for the introduction of these nanoparticles into the mesoporous silica structure.<sup>28</sup> Nonionic diblock copolymers (poly(butylene oxide)–poly(ethylene oxide)) and star diblock poly(ethylene oxide)–poly(propylene oxide) copolymers were also used in dilute acidic media to synthesize cubic mesoporous silicas and various mesoporous oxides.<sup>9,29,30</sup>

Some of the first reports on the application of polymeric templates also demonstrated that poly(alkylene oxide) triblock copolymers, such as poly(ethylene oxide)–poly(propylene oxide)–poly(ethylene oxide) (EO<sub>m</sub>PO<sub>n</sub>–EO<sub>m</sub>), are suitable templates for the synthesis of disordered mesoporous silicas<sup>2</sup> and aluminas in neutral media.<sup>3,4</sup> Later, the use of these templates in acidic media opened new opportunities in the synthesis of porous oxides,<sup>9,16,29–37</sup> thus paving an avenue to perhaps the most remarkable advances in the field of synthesis and application of polymer-templated porous oxides.<sup>9,16,29–44</sup> EO<sub>m</sub>PO<sub>n</sub>EO<sub>m</sub> and some other triblock copolymers were found to self-assemble with silicate species in acidic media to form periodic mesoporous silicas, including hexagonal structures (referred to as SBA-15) with ordered pores as large as 30 nm and cubic structures.<sup>9,31</sup> This methodology was extended to the synthesis of ordered large-pore mesoporous silica monoliths,<sup>9</sup> fibers,<sup>32</sup> ordered continuous mesoporous silica films,<sup>16,17</sup> hexagonal mesoporous silica rods,<sup>33</sup> spongelike membranes,<sup>34</sup> and spherical nanoparticles.<sup>17</sup> What is even more remarkable is that the application of triblock copolymers in nonaqueous media allowed for the successful preparation of periodic mesoporous oxides, such as TiO<sub>2</sub>, ZrO<sub>2</sub>, Al<sub>2</sub>O<sub>3</sub>, Nb<sub>2</sub>O<sub>5</sub>, Ta<sub>2</sub>O<sub>5</sub>, WO<sub>3</sub>, HfO<sub>2</sub>, and SnO<sub>2</sub>, as well as a variety of mixed oxides.<sup>29,30</sup> These triblock copolymer syntheses were combined with polystyrene sphere templating and micromolding to prepare hierarchically ordered oxides with porous systems independently tailored on three different length scales.<sup>35</sup> In addition, EO<sub>m</sub>PO<sub>n</sub>EO<sub>m</sub> triblock copolymers swollen by trimethylbenzene (TMB) were found useful for the synthesis of siliceous mesocellular foams (MCFs) with uniform cells and windows, which was later explained as the result of templating by copolymer/TMB microemulsions.<sup>37</sup> The hexagonal SBA-15 silica, which exhibits a remarkable hydrothermal stability<sup>9,31</sup> and can be synthesized in a wide range of pore sizes and particle morphologies,<sup>9,16,31–35</sup> has already been tested for several applications in the fields of catalysis, separations, and advanced optical materials. In particular, SBA-15 silicas functionalized via framework incorporation of Al<sup>38–40</sup> and Ti<sup>41</sup> heteroatoms as well as via chemical bonding of organosilanes<sup>42</sup> exhibited highly promising catalytic performance.<sup>38,40,42</sup> Organosilane-modified SBA-

(11) Bagshaw, S. A. *Stud. Surf. Sci. Catal.* **1998**, *117*, 381.

(12) Bagshaw, S. A. *Chem. Commun.* **1999**, 271.

(13) Sierra, L.; Guth J.-L. *Microporous Mesoporous Mater.* **1999**, *27*, 243.

(14) Kwon, O.-Y.; Kim, S.; Choi, S.-W. *Microporous Mesoporous Mater.* **1999**, *27*, 255.

(15) Boissiere, C.; van der Lee, A.; El Mansouri, A.; Larbot, A.; Prouzet, E. *Chem. Commun.* **1999**, 2047.

(16) Zhao, D.; Yang, P.; Melosh, N.; Feng, J.; Chmelka, B. F.; Stucky, G. D. *Adv. Mater.* **1998**, *10*, 1380.

(17) Lu, Y.; Fan, H.; Stump, A.; Ward, T. L.; Rieker, T.; Brinker, J. C. *Nature* **1999**, *398*, 223.

(18) Brinker, C. J.; Lu, Y.; Sellinger, A.; Fan, H. *Adv. Mater.* **1999**, *11*, 579.

(19) Richer, R.; Mercier, L. *Chem. Commun.* **1998**, 1775.

(20) Thieme, M.; Schuth, F. *Microporous Mesoporous Mater.* **1999**, *27*, 193.

(21) Prouzet, E.; Cot, F.; Nabias, G.; Larbot, A.; Kooyman, P.; Pinnavaia, T. J. *Chem. Mater.* **1999**, *11*, 1498.

(22) Weissenberg, M. C.; Goltner, C. G.; Antonietti, M. *Ber. Bunsenges. Phys. Chem.* **1997**, *101*, 1679.

(23) Goltner, C. G.; Henke, S.; Weissenberger, M. C.; Antonietti, M. *Angew. Chem., Int. Ed. Engl.* **1998**, *37*, 613.

(24) Kramer, E.; Forster, S.; Goltner, C.; Antonietti, M. *Langmuir* **1998**, *14*, 2027.

(25) Goltner, C. G.; Berton, B.; Kramer, E.; Antonietti, M. *Chem. Commun.* **1998**, 2287.

(26) Goltner, C. G.; Berton, B.; Kramer, E.; Antonietti, M. *Adv. Mater.* **1999**, *11*, 395.

(27) Antonietti, M.; Berton, B.; Goltner, C.; Hentze, H.-P. *Adv. Mater.* **1998**, *10*, 154.

(28) Bronstein, L.; Kramer, E.; Berton, B.; Burger, C.; Forster, S.; Antonietti, M. *Chem. Mater.* **1999**, *11*, 1402.

(29) Yang, P.; Zhao, D.; Margolese, D. I.; Chmelka, B. F.; Stucky, G. D. *Nature* **1998**, *396*, 152.

(30) Yang, P.; Zhao, D.; Margolese, D. I.; Chmelka, B. F.; Stucky, G. D. *Chem. Mater.* **1999**, *11*, 2813.

(31) Zhao, D.; Feng, J.; Huo, Q.; Melosh, N.; Fredrickson, G. H.; Chmelka, B. F.; Stucky, G. D. *Science* **1998**, *279*, 548.

(32) Yang, P.; Zhao, D.; Chmelka, B. F.; Stucky, G. D. *Chem. Mater.* **1998**, *10*, 2033.

(33) Schmidt-Winkel, P.; Yang, P.; Margolese, D. I.; Chmelka, B. F.; Stucky, G. D. *Adv. Mater.* **1999**, *11*, 303.

(34) Zhao, D.; Yang, P.; Chmelka, B. F.; Stucky, G. D. *Chem. Mater.* **1999**, *11*, 1174.

(35) Yang, P.; Deng, T.; Zhao, D.; Feng, P.; Pine, D.; Chmelka, B. F.; Whitesides, G. M.; Stucky, G. D. *Science* **1998**, *282*, 2244.

(36) Schmidt-Winkel, P.; Lukens, W. W., Jr.; Zhao, D.; Yang, P.; Chmelka, B. F.; Stucky, G. D. *J. Am. Chem. Soc.* **1999**, *121*, 254.

(37) Schmidt-Winkel, P.; Glinka, C. J.; Stucky, G. D. *Langmuir* **2000**, *16*, 356.

(38) Cheng, M.; Wang, Z.; Sakurai, K.; Kumata, F.; Saito, T.; Komatsu, T.; Yashima, T. *Chem. Lett.* **1999**, 131.

(39) Luan, Z.; Hartmann, M.; Zhao, D.; Zhou, W.; Kevan, L. *Chem. Mater.* **1999**, *11*, 1621.

(40) Yue, Y.; Gedeon, A.; Bonardet, J.-L.; Melosh, N.; D'Espinose, J.-B.; Fraissard, J. *Chem. Commun.* **1999**, 1967.

(41) Luan, Z.; Maes, E. M.; van der Heide, P. A. W.; Zhao, D.; Czernuszewicz, R. S.; Kevan, L. *Chem. Mater.* **1999**, *11*, 3680.

15 and MCFs were found useful in sequestration and release of proteins.<sup>43</sup> As-synthesized SBA-15 materials patterned using soft lithography were shown to be applicable as waveguides and, after doping, as mirror-lasers.<sup>44</sup>

Despite all of the aforementioned advances in the synthesis and application of oligomer- and polymer-templated oxides, and triblock-copolymer-templated silicas in particular, relatively little work was done in the direction of the comprehensive characterization of these important materials, although their structures are often quite complicated and far from being fully understood. In particular, some studies indicated the presence of microporosity in SBA-15<sup>45</sup> and other polymer-templated materials,<sup>26</sup> although the origin of microporosity and its location in the structure were not identified. Our preliminary study of SBA-15 confirmed the presence of a broad distribution of micropores/small mesopores, provided an estimate of their size range, suggested their origin, and demonstrated that they are located in the walls of the large ordered mesopores, providing connectivity between these pores.<sup>46</sup> In the current paper we describe results of detailed nitrogen adsorption, X-ray diffraction (XRD), and thermogravimetric analysis (TGA) characterization of uncalcined and calcined SBA-15. New evidence for the presence of complementary microporosity/mesoporosity in SBA-15 is presented, and some important aspects of the synthesis process and the resulting temperature dependence of the SBA-15 structure are discussed.

## Experimental Section

**Materials.** SBA-15 silicas were synthesized as reported by Zhao et al.<sup>9,31</sup> using Pluronic P123 triblock copolymer (EO<sub>20</sub>-PO<sub>70</sub>EO<sub>20</sub>). A 4.0 g sample of Pluronic P123 was dissolved in 30 g of water and 120 g of 2 M HCl solution. Then, 8.50 g of TEOS was added, and the resulting mixture was stirred for 5 min and then kept at 308 K for 20 h without stirring. Except for sample S0, this low-temperature preparation was followed by aging for 1 day at 353 K (sample S1), for 2 days at 353 K (sample S2), for 2 days at 363 K (sample S3), or for 2 days at 373 K (sample S4). The solid product was filtered, washed with water or ethanol, and dried in an oven for 4 h at 413 K. Because the washing led to a partial surfactant removal, one of the samples (S0) was also isolated without washing to obtain a material with the intact template. To completely remove the surfactant, the as-synthesized product was slurried in EtOH-HCl solution for 30 min, filtered, dried in an oven at 413 K, and subsequently calcined in air for 4 h at 823 K. The samples will be referred to as *Sn*-Y, where *n* and Y denote, respectively, the number (0–4) and type of the sample (A, as-synthesized, unwashed; W, as-synthesized, water-washed; E, as-synthesized, ethanol-washed; C, calcined).

**Measurements.** Powder XRD patterns were recorded on a Rigaku D/MAX-III diffractometer using Cu K $\alpha$  radiation. For the S0 sample, measurements were also carried out on a Siemens D5005 diffractometer to obtain more resolved XRD patterns at 2 $\theta$  angles from 1.5° to 5°. Nitrogen adsorption

measurements at 77 K were performed on an ASAP 2010 volumetric adsorption analyzer. Before the measurements, the samples were outgassed for 2 h in the degas port of the adsorption apparatus, at 473 K for the calcined samples and at 323 K for the ethanol- and water-washed samples. TGA measurements were carried out under flowing nitrogen on a TA Instruments TGA 2950 high-resolution thermogravimetric analyzer using a high-resolution mode with a maximum heating rate of 5 K min<sup>-1</sup>.

**Calculation Methods.** The BET specific surface area<sup>47</sup> was evaluated using adsorption data in a relative pressure range from 0.04 to 0.2. The total pore volume<sup>47</sup> was estimated from the amount adsorbed at a relative pressure of about 0.99. The external surface area,  $S_{\text{ex}}$ , primary mesopore volume,  $V_{\text{p}}$ , and micropore volume,  $V_{\text{mi}}$ , were evaluated using the  $\alpha_s$ -plot method, as described elsewhere.<sup>48</sup>  $V_{\text{mi}}$  was calculated using the standard reduced adsorption,  $\alpha_s$ , interval from 0.9 to 1.2 (relative pressure range from 0.3 to 0.58) for samples S1-C to S4-C, and from 0.75 to 1 (relative pressure range from 0.16 to 0.38) for sample S0-C. The volume of the primary mesopores and other mesopores/micropores of size smaller than that of the primary mesopores, and the external surface area were evaluated using  $\alpha_s$  from 1.8 to 2.5 for S1–S4 and S0-E samples, and from 1.5 to 2.0 for the S0-C sample. The primary mesopore volume was estimated as a difference between the pore volume mentioned above and the micropore volume. LiChrospher Si-1000 silica gel was used as a reference solid in the  $\alpha_s$ -plot analysis.<sup>49</sup> The mesopore size distribution (PSD) was calculated on the basis of adsorption branches of nitrogen isotherms using the BJH method with the corrected form of the Kelvin equation and the statistical film thickness curve, both determined using a series of MCM-41 materials, as reported by Kruk, Jaroniec, and Sayari.<sup>50</sup> The primary mesopore size,  $w_{\text{KJS}}$ , was defined as a maximum on the PSD calculated using the latter method. The pore wall thickness,  $b_{\text{KJS}}$ , was assessed by subtracting  $w_{\text{KJS}}$  from the distance between the centers of adjacent pores,  $a$ . The latter was evaluated from the (200) interplanar spacing,  $d_{200}$ , according to the following formula:  $a = 4 \times 3^{-1/2} d_{200}$ . The (200) interplanar spacing was used instead of the (100) interplanar spacing, because the XRD diffractometers used in the current study were not capable of reliably determining the position of peaks at 2 $\theta$  angles of about 1° or lower, where the (100) diffraction peaks were observed. The primary mesopore size of SBA-15 was also evaluated using a geometrical relation among the unit-cell size, pore volume, and pore size,  $w_{\text{d}}$ , in a honeycomb structure.<sup>51</sup>

$$w_{\text{d}} = cd \left( \frac{\rho V_{\text{p}}}{1 + \rho V_{\text{p}}} \right)^{1/2}$$

where  $c$  is a constant dependent on the pore geometry (1.213 for circular pores as well as for hexagonal pores, if the size of the latter is defined as the diameter of a circle of the same area as the hexagonal pore cross-section) and  $\rho$  is the pore wall density, assumed to be equal to that of amorphous silica, which is 2.2 g cm<sup>-3</sup>.<sup>51</sup> The XRD (100) interplanar spacing  $d$  in eq 1 was estimated from the XRD (200) interplanar spacing:  $d = 2d_{200}$ .

## Results and Discussion

**X-ray Diffraction.** Calcined SBA-15 silica prepared at low temperature (S0-C) exhibited a single strong peak on its XRD pattern (Figure 1). Similar patterns were recorded for the as-synthesized unwashed (S0-A) and

(42) Bae, S. J.; Kim, S.-W.; Hyeon, T.; Kim, B. M. *Chem. Commun.* **1999**, 31.

(43) Han, Y.-J.; Stucky, G. D.; Butler, A. J. *Am. Chem. Soc.* **1999**, *121*, 9897.

(44) Yang, P.; Wirnsberger, G.; Huang, H. C.; Cordero, S. R.; McGehee, M. D.; Scott, B.; Deng, T.; Whitesides, G. M.; Chmelka, B. F.; Buratto, S. K.; Stucky, G. D. *Science* **2000**, *287*, 465.

(45) Lukens, W. W., Jr.; Schmidt-Winkel, P.; Zhao, D.; Feng, J.; Stucky, G. D. *Langmuir* **1999**, *15*, 5403.

(46) Ryoo, R.; Ko, C. H.; Kruk, M.; Antochshuk, V.; Jaroniec, M. J. *Phys. Chem. B*, submitted for publication.

(47) Sing, K. S. W.; Everett, D. H.; Haul, R. A. W.; Moscou, L.; Pierotti, R. A.; Rouquerol, J.; Siemieniowska, T. *Pure Appl. Chem.* **1985**, *57*, 603.

(48) Sayari, A.; Liu, P.; Kruk, M.; Jaroniec, M. *Chem. Mater.* **1997**, *9*, 2499.

(49) Jaroniec, M.; Kruk, M.; Olivier, J. P. *Langmuir* **1999**, *15*, 5410.

(50) Kruk, M.; Jaroniec, M.; Sayari, A. *Langmuir* **1997**, *13*, 6267.

(51) Kruk, M.; Jaroniec, M.; Sayari, A. *Chem. Mater.* **1999**, *11*, 492.

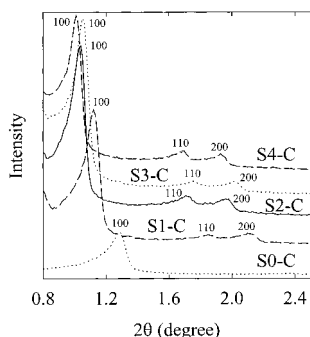


**Figure 1.** Powder X-ray diffraction patterns for the calcined SBA-15 samples.

ethanol-washed (S0-E) samples. To achieve better resolution of the higher-order reflections, the XRD patterns were recorded on another XRD spectrometer (Figure 1S in the Supporting Information). Two additional peaks were observed, which can be indexed on a hexagonal lattice as (200) and (210) reflections. The XRD patterns for S0 samples did not feature clear (110) reflections, although in the case of the calcined sample, there was some increase in intensity at  $2\theta$  angles, where this reflection would appear. The absence of well-pronounced (110) reflections was not surprising, since the reported XRD patterns of as-synthesized SBA-15 prepared at low temperature featured weak (110) peaks.<sup>9,31</sup> Anyway, it is apparent that the S0 SBA-15 sample under current study exhibited structural ordering somewhat lower than that of the material prepared by Zhao et al.<sup>9,31</sup> under similar conditions. The XRD unit-cell parameter of the S0 sample decreased significantly after the ethanol washing (from 10.4 to 9.2 nm) and subsequent calcination (to 8.3 nm). The shrinkage upon ethanol washing was somewhat unexpected, because MCM-41 and FSM-16 materials of hexagonal structures similar to that of SBA-15 often retained their unit-cell sizes after the low-temperature template removal, for instance via solvent extraction<sup>52,53</sup> or ozone treatment.<sup>54</sup> The possible reason for the peculiar behavior of SBA-15 will be discussed later.

XRD patterns of the calcined SBA-15 samples prepared at higher temperatures exhibited three clear peaks characteristic of hexagonally ordered structure (Figure 1). As in the case of the material prepared at lower temperature, the calcination caused appreciable decrease in the unit-cell size in comparison to that of the uncalcined samples (water-washed or ethanol-washed; see data in Tables 1 and 1S). Water-washed samples had unit-cell sizes larger than those of the ethanol-washed materials (as discussed later, washing with water removed smaller amounts of the polymer template).

Relative intensities of (110) and (200) peaks varied as the synthesis temperature was increased. As discussed above, the calcined SBA-15 sample prepared at low temperature exhibited strong (200) reflection, whereas the (110) reflection was hardly visible (Figure 1S). The sample aged at 353 K for 1 day (S1-C) also

**Table 1. Selected Structural Parameters of the SBA-15 Silicas<sup>a</sup>**

sample	<i>a</i> (nm)	<i>S</i> <sub>BET</sub> (m <sup>2</sup> /g)	<i>V</i> <sub>t</sub> (cm <sup>3</sup> /g)	<i>V</i> <sub>p</sub> (cm <sup>3</sup> /g)	<i>V</i> <sub>mi</sub> (cm <sup>3</sup> /g)	<i>S</i> <sub>ex</sub> (m <sup>2</sup> /g)
S0-E	9.2	400	0.42	0.38 <sup>b</sup>	<i>b</i>	20
S0-C	8.3	520	0.44	0.33	0.08	20
S1-W	11.1	510	0.65	0.62 <sup>b</sup>	<i>b</i>	20
S1-C	9.7	780	0.81	0.62	0.12	40
S2-W	11.3	630	0.82	0.77 <sup>b</sup>	<i>b</i>	40
S2-C	10.4	870	0.96	0.75	0.12	60
S3-W	11.5	580	0.88	0.81 <sup>b</sup>	<i>b</i>	40
S3-C	10.2	850	1.02	0.84	0.08	60
S4-W	11.2	550	0.87	0.81 <sup>b</sup>	<i>b</i>	40
S4-C	10.6	850	1.08	0.92	0.06	70

<sup>a</sup> *a*, XRD unit-cell parameter; *S*<sub>BET</sub>, BET specific surface area; *V*<sub>t</sub>, total pore volume; *V*<sub>p</sub>, primary mesopore volume evaluated using the  $\alpha_s$ -plot method (*V*<sub>p</sub> includes a certain contribution from the volume of the complementary pores, so the actual primary mesopore volume is smaller); *V*<sub>mi</sub>, micropore volume; *S*<sub>ex</sub>, external surface area. <sup>b</sup> Because of the differences in low-pressure nitrogen adsorption properties between the reference silica and polymer-containing water-washed materials, the micropore volume cannot be reliably determined using the  $\alpha_s$ -plot method with such a reference sample. Consequently, *V*<sub>p</sub> may include a contribution from the volume of complementary pores.

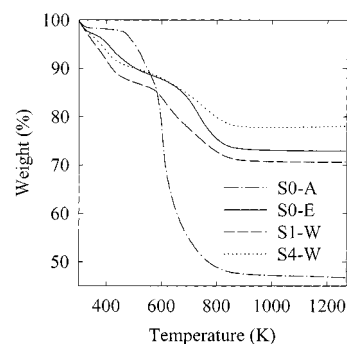


**Figure 2.** Weight change curves for selected SBA-15 samples.

exhibited (200) reflection more intense than the (110) reflection, but the opposite was true for the sample aged at 373 K (S4-C) (Figure 1). Similar differences in relative peak intensities were also observed for water- and ethanol-washed samples. Such changes in relative intensity of (110) and (200) peaks have already been discussed in the literature in the case of MCM-41,<sup>51,55,56</sup> and it was shown that the samples with thicker pore walls exhibit larger relative intensities of (200) peaks. Our pore wall thickness estimates (see below) confirmed that the pore wall thickness (relative to the unit-cell size) tends to decrease as the relative intensity of the (200) peak to the (110) peak decreases.

**Thermogravimetry.** The as-synthesized unwashed S0-A sample exhibited about 50% TGA weight loss at temperatures between 373 and 923 K (Figure 2). This weight loss can be attributed primarily to the decomposition and desorption of the polymeric template and, to a smaller extent, to the release of water formed from the condensation of silanols in the silica framework. The content of the polymeric template in this SBA-15 sample was similar to the content of the ionic surfactant template in typical MCM-41 and MCM-48 silicas.<sup>57,58</sup>

(52) Kawi, S.; Lai, M. W. *Chem. Commun.* **1998**, 1407.

(53) Inagaki, S.; Sakamoto, Y.; Fukushima, Y.; Terasaki, O. *Chem. Mater.* **1996**, *8*, 2089.

(54) Keene, M. T. J.; Denoyal, R.; Llewellyn, P. L. *Chem. Commun.* **1998**, 2203.

(55) Feuston, B. P.; Higgins, J. B. *J. Phys. Chem. B* **1994**, *98*, 4459.

(56) Agren, P.; Linden, M.; Rosenholm, J. B.; Schwarzenbacher, R.; Kriechbaum, M.; Amenitsch, H.; Laggner, P.; Blanchard, J.; Schuth, F. *J. Phys. Chem. B* **1999**, *103*, 5943.

(57) Kruk, M.; Sayari, A.; Jaroniec, M. *Stud. Surf. Sci. Catal.* **2000**, *129*, 577.

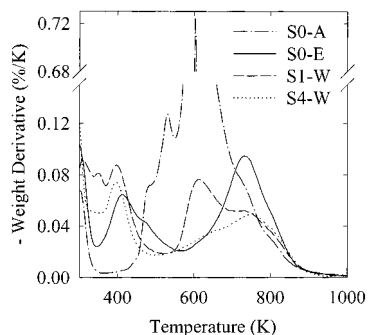


**Figure 3.** Weight change derivatives for selected SBA-15 samples.

It is interesting that, under nitrogen atmosphere, the decomposition of the polymeric template took place at relatively high temperatures (maximum on the weight loss derivative at about 600 K; see Figure 3) and the template seemed to be partially retained to yet much higher temperatures (at least 800 K). In nitrogen atmosphere, ionic surfactant templates in pure-silica materials usually decompose essentially completely at much lower temperatures (below 600 K).<sup>57,58</sup> The high decomposition temperature of the polymeric template under nitrogen atmosphere is in contrast to the decomposition under air atmosphere, where most of the template was removed below 500 K.<sup>31</sup>

After the ethanol washing, the content of the polymeric template decreased significantly, yet about 20% of the polymer was present in the S0-E sample, as inferred from the weight loss between 373 and 923 K (Figure 2). In this case a part of the template was also retained up to relatively high temperature (750 K). A similar behavior was observed for other water-washed and ethanol-washed samples (see Figures 2 and 3). Namely, the polymeric template exhibited a broad range of decomposition temperatures and was retained up to about 900 K, since the weight losses at temperatures between 600 and 900 K were too high to be solely attributed to the release of water from condensation of silanols. In most cases, the percentage of the template left in the structure after water and ethanol washing decreased as the synthesis/aging temperature for a given sample increased (see for instance Figure 2), and the water-washed samples retained more template than the ethanol-washed samples.

**Nitrogen Adsorption.** Nitrogen adsorption isotherms for the calcined SBA-15 samples under study (Figure 4) are similar to those reported earlier<sup>9,31</sup> and characteristic of good-quality SBA-15. Similarly to the nitrogen adsorption isotherms for large-pore MCM-41,<sup>48,50,59</sup> the isotherms of SBA-15 samples featured hysteresis loops with sharp adsorption and desorption branches. The sharpness of the adsorption branches is indicative of a narrow mesopore size distribution. The adsorption branches were located at relative pressures in the range from 0.55 to 0.8, which includes relative pressures higher than those for good-quality MCM-41 materials (up to 0.7).<sup>48,50,59</sup> The positions of the adsorption branches for SBA-15 shifted toward higher pres-

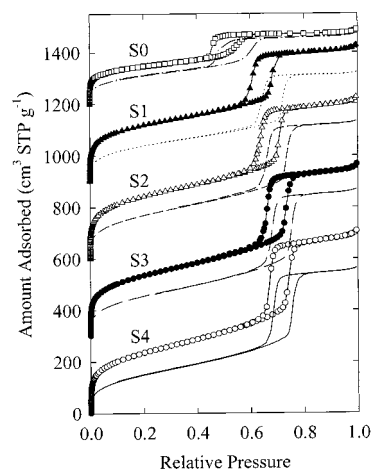


**Figure 4.** Nitrogen adsorption isotherms for the SBA-15 silicas. The adsorption isotherms for S3, S2, S1, and S0 samples are shifted by 300, 600, 900, and 1200 cm<sup>3</sup> STP g<sup>-1</sup>, respectively. Lines with symbols show adsorption data for calcined samples, whereas lines without symbols show data for water-washed (S1–S4) or ethanol-washed (S0) samples.

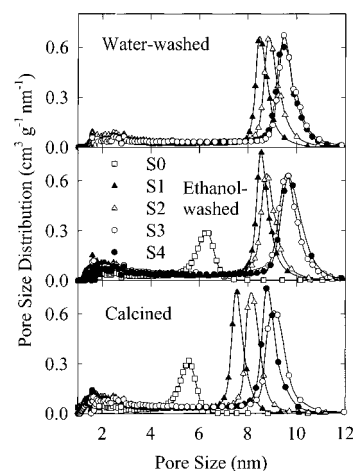


**Figure 5.** Pore size distributions for the SBA-15 silicas.

ures as the synthesis temperature increased. Since the capillary condensation pressure is an increasing function of the pore diameter,<sup>47,50</sup> the observed behavior confirms that the pore size of SBA-15 can be tailored by a judicious choice of the synthesis/aging temperature, as reported before.<sup>9,31</sup> The pore size distributions (PSDs) for the calcined SBA-15 samples are shown in Figure 5, and the pore sizes corresponding to their maxima are listed in Table 1. The PSDs exhibited sharp maxima for pore sizes between 5.5 and 9 nm. Similar primary mesopore sizes were evaluated using eq 1, which was derived for materials with honeycomb structures. The pore sizes, BET specific surface areas, and total pore volumes of SBA-15 samples under current study were in good agreement with those previously reported by Zhao et al.<sup>9,31</sup> It should be noted that the aforementioned authors calculated pore sizes from adsorption branches of isotherms, as was done in the current study, but used the Kelvin equation with the statistical film thickness correction, which may lead to the pore diameter underestimation of about 1 nm in the pore size range considered.<sup>50</sup> Consequently, the SBA-15 pore wall thickness reported previously might have been overestimated by about 1 nm, thus being probably below about 3 nm

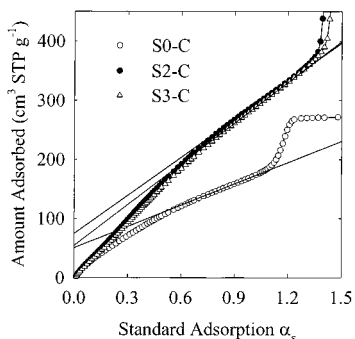
(58) Kruk, M.; Jaroniec, M.; Ryoo, R.; Joo, S. H. *Chem. Mater.* **2000**, *12*, 1414.

(59) Huo, Q.; Margolese, D. I.; Stucky, G. D. *Chem. Mater.* **1996**, *8*, 1147.

**Table 2. Pore Sizes and Pore Wall Thicknesses of SBA-15 Silicas<sup>a</sup>**

sample	$w_{\text{KJS}}$ (nm)	$w_{\text{d}}$ (nm)	$b_{\text{KJS}}$ (nm)	$b_{\text{d}}$ (nm)
S0-E	6.3		2.9	
S0-C	5.6	5.7	2.7	2.7
S1-W	8.5		2.6	
S1-C	7.6	7.7	2.1	2.0
S2-W	8.9		2.4	
S2-C	8.1	8.6	2.3	1.8
S3-W	9.5		2.0	
S3-C	8.8	8.6	1.4	1.6
S4-W	9.5		1.7	
S4-C	9.0	9.1	1.6	1.5

<sup>a</sup>  $w_{\text{d}}$  and  $b_{\text{d}}$ , pore diameter and pore wall thickness calculated on the basis of eq 1;  $w_{\text{BJH}}$  and  $b_{\text{BJH}}$ , pore diameter and pore wall thickness calculated on the basis of the KJS approach.

**Figure 6.**  $\alpha_s$  plots for selected calcined SBA-15 silicas.

in the case of the materials synthesized under conditions employed in the current study (see Table 2). Our study shows that some SBA-15 samples may even exhibit pore wall thickness comparable to those of MCM-41 samples with very thick pore walls obtained in high-temperature conditions.<sup>48</sup> This in turn suggests that an exceptional hydrothermal stability of SBA-15 may be caused by not only the large pore wall thickness,<sup>9,31</sup> but also some other factors.

In addition to the narrow distribution of large mesopores, the SBA-15 samples exhibited a wide range of smaller pores with a broad maximum at about 2 nm.<sup>46</sup> The presence of micropores was also evident from the  $\alpha_s$ -plot analysis.<sup>46</sup> As seen in Figure 6, the initial parts of  $\alpha_s$  plots for the calcined SBA-15 samples were significantly nonlinear, in contrast to the  $\alpha_s$  plots for calcined MCM-41 and other nonmicroporous silicas, which usually exhibit excellent linearity in the low-pressure range (see for instance refs 48–50, 58, and 60). The micropore volumes assessed using the  $\alpha_s$ -plot method ranged from 0.06 to 0.12 cm<sup>3</sup> g<sup>-1</sup>. However, it needs to be kept in mind that the PSD calculations indicated the presence of a small amount of mesopores of size below 6 nm. The latter exhibit capillary condensation at relative pressures below 0.6,<sup>50</sup> that is, within the relative pressure ranges used in the  $\alpha_s$ -plot analysis to assess the micropore volume. Consequently, the resulting micropore volume may be somewhat underestimated, and the primary mesopore volume (which is evaluated using the micropore volume) may be overestimated.

Our previous study provided a direct confirmation that a significant fraction of the complementary pores of SBA-15 exhibit sizes in an approximate range from 1 to 3 nm.<sup>46</sup> This was inferred from the fact that the chemical modification of the SBA-15 surface using

relatively small trimethylsilyl ligands led to the decrease in the primary mesopore size of SBA-15 by about 0.8 nm, but yet resulted only in a partial blockage of the complementary pores (as demonstrated by examining the relation among the pore size, pore volume, and specific surface area). On the other hand, the complementary pores were successfully blocked after modification with rather large octyldimethylsilyl ligands, which led to the primary mesopore size decrease by about 1.8 nm (the maximum pore diameter decrease, which can result from a dense packing of fully extended  $-\text{Si}(\text{CH}_3)_2\text{C}_8\text{H}_{17}$  ligands, can be estimated on the basis of the bond lengths/angles as about 2.6 nm). Since the size of the nitrogen molecule is about 0.35 nm,<sup>61</sup> the result of the modification with TMS provided evidence that the SBA-15 sample under study had a considerable fraction of complementary pores of the size above 1.2 nm. After the modification, such pores would have a size above 0.4 nm, and therefore would still be potentially accessible for nitrogen, provided there would be no pore connectivity effects, which would restrict the access of nitrogen to these pores. In addition, the results of the modification with ODMS demonstrated that most of the complementary pores were of size below 3 nm or were connected with the surrounding pores via constrictions of size below 3 nm, since the ODMS ligands would not be able to block the access of nitrogen to wider pores.

In addition to the determination of the pore size range characteristic of the complementary pores, their location in the SBA-15 structure was elucidated by examining the platinum replica of the SBA-15 pores prepared via platinum deposition and dissolution of the silica framework.<sup>46</sup> The replica consisted of bunches of platinum wires of size corresponding to the primary mesopores of SBA-15. The wires exhibited a long-range structural ordering, which provided direct evidence of their connectivity, whereas no long-range ordering was observed for platinum replicas of the MCM-41 structure. Therefore, it was inferred that the complementary pores provide connectivity between the primary mesopores of SBA-15,<sup>46</sup> although the determination of the relative amount of the connecting pores will require further studies. The total volumes of the complementary pores were estimated from the PSD analysis as about 0.25 cm<sup>3</sup> g<sup>-1</sup> for samples S1-C to S4-C and about half of this amount for the S0-C material. These pores exhibited a broad size distribution, as discussed above, but in general this distribution tended to shift slightly to the larger pore sizes as the synthesis/aging temperature increased. This is clear from the  $\alpha_s$ -plot analysis, because the plot for the calcined SBA-15 sample prepared at low temperature was strongly nonlinear and clearly characteristic of the microporous–mesoporous materials, whereas the plots for the other calcined samples exhibited better linearity (see Figure 6 and ref 46). This can be explained as an effect of the increase in size of the complementary pores and/or broadening of their size distribution toward the mesopore range. It should be noted here that the presence of microporosity in SBA-15 was indicated by the studies of Lukens et al.<sup>45</sup> However, their conclusions were based on calcula-

(60) Kruk, M.; Jaroniec, M.; Sakamoto, Y.; Terasaki, O.; Ryoo, R.; Ko, C. H. *J. Phys. Chem. B* **2000**, *104*, 292.

(61) Gregg, S. J.; Sing, K. S. W. *Adsorption, Surface Area and Porosity*; Academic Press: London, 1982.

tions performed using reference adsorption data for quartz, which is a crystalline silica. It is well-known that the degree of crystallinity may have a considerable impact on the adsorption properties of materials. This is evident for porous carbons, whose adsorption properties change dramatically with the change in the degree of graphitization,<sup>61,62</sup> and consequently graphitized carbons are not good as reference adsorbents for studies of nongraphitized carbons.<sup>62</sup> Therefore, it is doubtful that the adsorption isotherm for quartz is adequate as a reference adsorption isotherm for the characterization of amorphous silicas. One can conclude that the data for quartz should not be used in the  $\alpha_s$ -plot analysis of amorphous silicas, unless their applicability is carefully examined and confirmed. It also needs to be kept in mind that good reference nitrogen and argon adsorption isotherm data for amorphous silicas are available in the scientific literature,<sup>49,61,63</sup> including reliable low-pressure data, which were not available until recently.<sup>49,63</sup>

It was reported by Zhao et al.<sup>34</sup> that water-washed SBA-15 spongelike membranes had accessible primary mesopores, which was explained as a result of an appreciable removal of the polymer template during the water washing. Our study confirmed this finding, since nitrogen adsorption isotherms for water-washed SBA-15 samples are similar to those of the corresponding calcined samples (Figure 4). The water-washed materials exhibited 14–20% lower total pore volumes, 28–35% lower BET specific surface areas (Table 1), and larger primary mesopore sizes (0.5–0.9 nm larger; see Table 2 and Figure 5). The lower pore volumes and specific surface areas are attributable to the presence of a certain amount of the copolymer in the water-washed structure (it was verified using TGA that the outgassing procedure used to prepare the samples for adsorption measurements did not lead to any appreciable loss of the polymeric template left after the washing). The fact that the differences in the specific surface areas were much larger than those in the total pore volumes indicated that pores of relatively high surface area/pore volume ratio were not accessible in the structure of the water-washed materials. Since high surface area/pore volume ratios are realized for narrow pores, one can expect that these were not the primary mesopores, but the complementary pores, which were preferentially occupied by the polymer template retained after the washing. This is consistent with the relatively large pore sizes for the water-washed samples, which were actually appreciably larger than those of the calcined samples (see Table 2 and Figure 5). This behavior can be attributed to the larger unit-cell sizes of the water-washed materials (Table 1), but still the presence of a considerable amount of the polymer template on the pore walls would offset the effect of the larger unit-cell size. As mentioned above, this was not observed, so the conclusion about the preferential location of the polymer in the complementary pores of the water-washed materials appears to be fully substantiated. Behavior similar to that of the water-washed materials was also observed for ethanol-washed samples (see Figures 4 and 2S), but the ethanol washing usually resulted in the removal of larger amounts of the polymer template. It

is interesting that, in some cases, adsorption capacities and, consequently, total pore volumes of the ethanol-washed samples exceeded those of the corresponding calcined materials (see Tables 1 and 1S). This peculiar behavior resulted from the fact that the effect of the larger unit-cell size surpassed the effects of the presence of the residual amounts of the polymer in the porous structure. The ethanol-washed samples also exhibited pore sizes larger than those of the calcined samples and similar to those of the water-washed materials. The latter usually contained larger amounts of the polymer template, but had slightly larger unit-cell parameters. The interplay between these two factors resulted in the highly similar pore sizes of the water-washed and ethanol-washed SBA-15 materials (see Figure 5).

**Explanation of the Occurrence of the Complementary Porosity as a Result of Properties of Triblock Copolymer Templates.** It is well-known that  $EO_mPO_nEO_m$  triblock copolymers in water form micelles, in which the core and mantle are composed of PO blocks and EO blocks, respectively.<sup>64–66</sup> At the temperatures used in the synthesis of SBA-15 samples under study (that is, 308–373 K), the PO block is strongly hydrophobic, whereas the hydrophobicity of the EO block strongly increases as temperature increases.<sup>64–66</sup> Thus, the PO block is not appreciably hydrated, whereas the degree of hydration of the EO block dramatically decreases at elevated temperatures. At lower temperatures, the poly(ethylene oxide) chains are surrounded by water molecules,<sup>64</sup> and as the temperature is increased, the EO chains tend to interact with fewer water molecules.<sup>64–66</sup> It is suggested that, in the case of SBA-15 materials prepared at low temperature (308 K), the silica framework is templated by triblock copolymer micelles with appreciably extended EO blocks, and thus it may be penetrated by these blocks. This is consistent with the recent studies of organoaluminosilicates templated by diblock copolymers with EO blocks<sup>67</sup> and monolytic silica-triblock copolymer composites.<sup>68</sup> These studies showed that EO blocks penetrate the frameworks of the templated organoaluminosilicate and silica materials. Thus, the calcined SBA-15 is likely to exhibit complementary micropores/mesopores in the parts of the framework where once the EO blocks were located, provided these voids are not eliminated or blocked as a result of framework condensation upon calcination.

It is known that dehydration of EO blocks takes place at higher temperatures.<sup>5,9,31,64–66</sup> This may lead to the redistribution of the EO blocks from the silica framework to the region adjacent to the cores of the micelles and/or to the aggregation of the EO blocks within the silica structure. Probably both of these mechanisms are operative, since our study showed that, as the synthesis/aging temperature increased, the volume of the complementary pores decreased only slightly relative to the primary mesopore volume, and yet the relative amount

(62) Kruk, M.; Jaroniec, M.; Choma, J. *Carbon* **1998**, *36*, 1447.

(63) Kruk, M.; Jaroniec, M. *Chem. Mater.* **2000**, *12*, 222.

(64) Wanka, G.; Hoffman, H.; Ulbricht, W. *Macromolecules* **1994**, *27*, 4145.

(65) Alexandridis, P.; Hatton, T. A. *Colloids Surf., A* **1995**, *96*, 1.

(66) Almgren, M.; Brown, W.; Hvidt, S. *Colloid Polym. Sci.* **1995**, *273*, 2.

(67) De Paul, S. M.; Zwanziger, J. W.; Ulrich, R.; Wiesner, U.; Spiess, H. W. *J. Am. Chem. Soc.* **1999**, *121*, 5727.

(68) Melosh, N. A.; Lipic, P.; Bates, F. S.; Wudl, F.; Stucky, G. D.; Fredrickson, G. H.; Chmelka, B. F. *Macromolecules* **1999**, *32*, 4332.

of the micropore volume decreased significantly. The fact of the penetration of EO blocks in the silica walls of as-synthesized SBA-15 provides an explanation of the appreciable unit-cell size contraction upon washing. It is suggested that the washing not only removes the polymer template which occupies the primary mesopores, but also reduces the amount of the EO blocks in the silica walls, which in turn creates void spaces in the walls, thus promoting the structural shrinkage. The increase in the pore size and the decrease in the pore wall thickness as temperature increases have already been explained by others<sup>5,9,31</sup> as results of the increasing hydrophobicity of the EO blocks, which led to the increased hydrophobic domain volumes and reduced length of EO segments interacting with the pore walls.

It is also important to note that although Pluronic triblock copolymers are characterized by a certain formula and average molecular weight, they are known to be polydisperse mixtures of triblock copolymers with a wide range of molecular weights.<sup>64–66</sup> They are also known to contain appreciable amounts of EO–PO diblock copolymers<sup>64–66</sup> and even free PO chains.<sup>66</sup> Some of these components, presumably the low-molecular-weight ones, may not be involved in the templating of the ordered porous domains of SBA-15, but may still act as templates for some disordered domains. Therefore, there is a distinct possibility that SBA-15 contains disordered domains templated by impurities present in the triblock copolymer used. These disordered domains would constitute another kind of complementary porosity of SBA-15, in addition to the pores that connect the large hexagonally ordered mesopores. The presence of

these connecting pores is evident from the TEM data, as already discussed, but so far there is no direct evidence of the presence of the aforementioned disordered domains. However, one can hardly envision that such significant volumes of the complementary pores as those revealed by our studies (the current study and ref 46) may be located solely in the pore walls, even though the latter are quite thick. Moreover, the recent study of monolytic silicas templated by triblock copolymer surfactant clearly demonstrated that different ordered phases may coexist in these materials.<sup>69</sup> Thus, the existence of disordered mesostructured impurity domains in SBA-15 is a distinct possibility.

**Acknowledgment.** Dr. S. D. Huang and Mr. C. Liu (Kent State University) are acknowledged for help in XRD measurements. The donors of the Petroleum Research Fund, administered by the American Chemical Society, are gratefully acknowledged for partial support of this research.

**Supporting Information Available:** Table 1S listing structural parameters assessed from XRD and nitrogen adsorption measurements and Figures 1S and 2S showing experimental data for XRD and nitrogen adsorption. This material is available free of charge via the Internet at <http://pubs.acs.org>.

CM000164E

---

(69) Melosh, N. A.; Davidson, P.; Chmelka, B. F. *J. Am. Chem. Soc.* **2000**, *122*, 823.